Saturation of the Electron-Withdrawing Capability of the NO_2 Group in Nitroaromatic Anions: Spectroscopic and Quantum-Chemical Evidence

Rômulo A. Ando, Antônio C. Borin, and Paulo S. Santos*

Instituto de Química, Universidade de São Paulo, Av. Prof. Lineu Prestes, 748 São Paulo, SP05508-000, Brazil

Received: March 15, 2007; In Final Form: May 7, 2007

The electronic (UV−vis) and resonance Raman (RR) spectra of the anionic species derived from 4-nitrophenol (pNP) and 4-nitroaniline (pNA) are reported. The interpretation of the electronic transitions in the visible, near-UV region was supported by quantum-mechanical calculations, allowing a consistent analysis of the enhancement patterns observed in the RR spectra, which show substantial differences in relation to those observed for the neutral species. The removal of the proton of the donor groups (OH and NH_2) leads to additional charge density at the oxygen atoms of the electron-withdrawing group (NO_2). On the other hand, when the RR spectra of $[pNP]^-$ and $[pNA]^-$ are compared, a drastic difference concerning the enhancement of modes related to the NO_2 moiety is noticed. In particular, in the case of $[pNA]^-$, the RR enhancement pattern involving the NO_2 moiety is at variance with those observed for nitroaromatics in general, because the corresponding normal modes involve a more complex composition. Such results are in accordance with the quantum-chemical calculations, which indicate, in the case of $[pNA]^-$, a saturation of the charge density at the N−O bonds, even in the ground state (i.e., the charge density is very similar in the ground and excited-state, which precludes large geometric variations of the NO_2 moiety in the two electronic states). Conversely, in this case the most enhanced bands have significant participation of ring modes, which suggests that the charge in the excited-state is now much more distributed in the molecule as a whole.

1. Introduction

Nitroaromatics were one of the first classes of molecules to deserve detailed investigations regarding the resonance Raman (RR) effect. In fact, the study of a series of nitroderivatives by Shorygin[1] reported an enhancement factor of ca. 10^3 in the intensity of the symmetric stretching of the NO_2 group ($\nu_s(NO_2)$) on going from nitropropane to *N*,*N*′-dimethyl-4-nitroaniline. In particular, the enhancement factor for the 4-nitrophenolate anion is striking at ca. 10^4. Over the years, many studies have been reported on the RR effect of nitroaromatics,[2−4] most of them motivated by the potential nonlinear optical properties of such materials.[5−9] One of the strategies used to optimize the nonlinear optical properties of push−pull molecules has been to increase the conjugation length along with the use of more efficient electron-donor and electron-withdrawing groups. In several 4-substituted nitroaromatics it is possible to obtain the corresponding anionic species via the deprotonation of acidic protons of groups such as OH or NH_2. The extra charge present in such species requires an extended electronic delocalization, reflected by a very substantial red-shift of the electronic transition and generally higher intensities when the proton is removed.

In ref 10, a time dependent density functional theory (TD−DFT) was applied to calculate the main geometric parameters of the archetypical push−pull chromophore 4-nitroaniline (pNA) in the ground state and in the intramolecular charge-transfer (CT) state, both in the gas phase and in solutions of different solvents. In particular, the N−O bond length increases from 1.235 to 1.307 Å upon excitation from the ground to the CT state. In fact, using the data for the geometric variations in pNA, one obtains a $\Delta r/r$ of ca. 6% for r(N−O), −2% for r(C−NH_2), −0.9% for r(C−NO_2), and −0.6% for r(C═C) (i.e., the N−O bond length is by far the most affected geometric parameter of pNA upon exciting the molecule to the CT state). Such substantial variation in the r(N−O) in going from the ground to the excited-state brings important consequences. In particular, a significant difference in electric dipole moments is expected, as has been determined experimentally[11−14] and calculated,[10,15,16] and this is the main reason for the solvatochromic behavior of pNA and related species. In addition, it is well known that the main source of the RR enhancement comes from the so-called Franck−Condon mechanism,[17] which implies a significant variation of one or more equilibrium bond lengths of the molecular moiety that constitutes the chromophoric unit involved in the electronic transition. Consequently, the Raman intensity is a property that depends on both ground and excited-state parameters. In this respect, the huge Raman enhancement observed for the $\nu_s(NO_2)$ mode in several nitroaromatics strongly suggests that this molecular moiety undergoes substantial variations in its geometry when excited to the resonant-state.

On the other hand, when one compares the available geometric parameters of 4-nitrophenol (pNP) and its anion ($[pNP]^-$), there are several interesting points . There are significant variations in the bond lengths of the C−O and N−O bonds, with the former becoming shorter and the latter becoming longer after deprotonation. It is well known that acidic species such as pNP become substantially more acidic in the excited-state,[18] which suggests that pNP in its excited-state has a structure that resembles its anion in the ground state. Obviously, without the geometry of the anion in the excited-state, it is not possible to make any prediction of the RR pattern for such species. In a previous publication,[19] the Raman and surface enhanced Raman scattering (SERS) spectra of pNA at several pH values were reported with emphasis on the adsorption geometry of the neutral and anionic species on the metal surface. The author proposes a loss of the ring aromaticity with the formation of a quinoid structure in the $[pNA]^-$ anion, which is responsible for the effective negative charge dispersing in the molecule.

In the case of the anions of pNP and pNA, one should expect higher charge density at the NO_2 group, even in the ground state. Consequently, the geometric variations of the NO_2 moiety

* To whom correspondence should be addressed. E-mail: pssantos@quim.iq.usp.br; phone: 55-11-30913853; fax: 55-11-30913890.

10.1021/jp072097i CCC: $37.00
Published on Web 07/12/2007

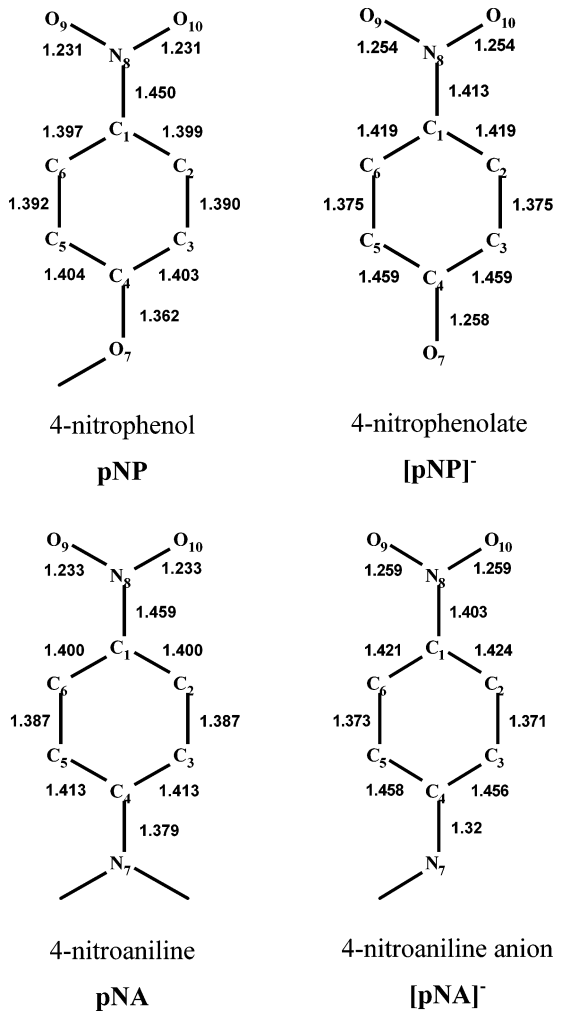

Figure 1. Structure of the investigated species, with the corresponding atoms numbering and the calculated interatomic distances and angles.

in the excited-state should be considerably smaller than those observed for the corresponding neutral species. If this is the case, one should then expect a different pattern of the resonance enhancement for the anions, as compared to those observed for the neutral species. In other words, if for the anions the charge density at the NO_2 group is already substantial in the ground state, then even powerful electron-donors such as O^- and NH^- will be much less effective in transferring extra charge to the NO_2 group because the electron-withdrawing group would be more or less saturated in its ability to accept additional charge density.

This was essentially the motivation that led us to undertake a detailed RR investigation of the model D-π-A systems, pNP, pNA, and their anions, supported by quantum-mechanical calculations for the geometries, charge densities, vibrational assignments, nature, and energies of the relevant electronic excitations for the investigated species. The para substituted species were chosen because the interpretation of vibrational spectra of the ortho substituted molecules is much more complex. On the other hand, the meta derivatives display a rather weak and noisy Raman spectra, and even in extremely basic solutions (pH ca. 26) the deprotonation equilibrium is almost completely displaced toward the neutral species, as expected from the much lower efficiency of the NO_2 group in the meta position to disperse the extra negative charge.

2. Experimental Section

All the reagents and solvents obtained from Aldrich were purified when necessary. The solutions of pNP, pNA, and their respective anions ($[pNP]^-$ and $[pNA]^-$) were prepared in suitable solvents. The neutral and anionic species of pNP ($pK_a = 7.15$) were studied in acidic and basic aqueous solution using 1 M $HCl_{(aq)}$ and 1 M $KOH_{(aq)}$, respectively. In the case of pNA ($pK_a = 18.9$), the deprotonation is achieved in an alkaline ($[OH^-] = 0.011$ M) aqueous/dimethyl-sulfoxide (DMSO) solution (99.6% mol of DMSO and 0.4% mol water, pH = 26.2).[20,21]

The UV−vis spectra were obtained on a Shimadzu UVPC-3101 spectrophotometer using quartz cells with a 1 mm optical path. The Raman spectra, excited by several lines of Ar^+ and Kr^+ lasers (Coherent INNOVA 90−6) ranging from 364 − 647 nm, were obtained in a Jobin-Yvon U1000 double spectrometer with photomultiplier detection (RCA-A02 at −20 °C). To avoid local heating, the sample was contained in a small NMR tube coupled to a rotator shaft. In the case of the nitrophenol solutions, the ca. 982 cm^{-1} Raman band of potassium sulfate (K_2SO_4) was used as internal standard, whereas in the case of the nitroaniline solutions, the DMSO band at 667 cm^{-1} was used as an internal standard. In the treatment of the Raman data, the fluorescence emission background was suppressed by applying smooth baseline corrections (Grams/32 AI 6.00).

Theoretical Methods. The ground state geometries of pNP, $[pNP]^-$, pNA, and $[pNA]^-$ were fully optimized by employing DFT with the B3LYP[22,23] hybrid functional (Becke's gradient-corrected exchange correlation in conjunction with the Lee−Yang−Parr correlation functional with three parameters) and the so-called aug-cc-pVDZ basis sets (augmented correlation consistent polarized valence double-ζ).[24] For pNP, $[pNP]^-$, and $[pNA]^-$, the nuclear framework was assumed to be planar (C_s point group symmetry) with the molecules located in the *xy* plane. In the case of pNA, the geometry were optimized without imposing any nuclear framework symmetry (C_1 point group). Vibrational frequency analysis was performed at the same level, and no imaginary frequencies were found. Geometry optimization and vibrational frequency analysis was carried out using the GAUSSIAN 03 software.[25]

The vertical electronic spectra were computed by employing the CASSCF/CASPT2 protocol (complete active space (CAS) self-consistent field (SCF) and multiconfigurational second-order perturbation (CASPT2))[26−28] with the shifted zero-order Hamiltonian proposed by Ghigo, Roos, and Malmqvist (IPEA)[29] (shift parameter of 0.25 hartree) and ANO (atomic natural orbital) basis sets[30] type of double-ζ with polarization (DZP) quality. The CASSCF/CASPT2 protocol has been applied successfully in several situations, with either inorganic or organic compounds.[31−33] The B3LYP optimized geometries obtained as described above were employed. The carbon, nitrogen, and oxygen core orbitals were kept frozen, and all π and π^* molecular orbitals were included in the active space, with the remaining molecular orbitals kept in the inactive space. Intruder states interacting weakly with the reference functions were removed using an imaginary shift of 0.1 hartree (imaginary level shift).[34] The reference functions were built by averaging over the first five lowest lying[1] (π, π^*) electronic states. The CASSCF/CASPT2 calculations were carried out with the MOLCAS 6.4 computational package.[35]

3. Results and Discussion

Figure 1 shows the structures of the investigated species with the corresponding atom numbering and the calculated inter-

TABLE 1: Calculated and Experimental Bond Lengths and Angles of pNP, [pNP]$^-$, pNA, and [pNA]$^-$

pNP						[pNP]$^-$					
	distance (Å)			distance (Å)			distance (Å)			distance (Å)	
bond	exp	calc	bond	exp	calc	bond	exp	calc	bond	exp	calc
C_1-C_2	1.394	1.399	C_6-C_1	1.393	1.397	C_1-C_2	1.418	1.419	C_6-C_1	1.322	1.419
C_2-C_3	1.378	1.390	C_5-C_6	1.382	1.392	C_2-C_3	1.358	1.375	C_5-C_6	1.358	1.375
C_3-C_4	1.399	1.403	C_4-C_5	1.396	1.404	C_3-C_4	1.409	1.459	C_4-C_5	1.427	1.459
C_1-N_8	1.450	1.404	N_8-O_9	1.243	1.231	C_1-N_8	1.430	1.413	N_8-O_9	1.253	1.254
C_4-O_7	1.361	1.362	N_8-O_{10}	1.241	1.231	C_4-O_7	1.295	1.258	N_8-O_{10}	1.238	1.254
	angle			angle			angle			angle	
	exp	calc		exp			exp	calc		exp	calc
$C_6-C_1-C_2$	122.0	121.5	$C_3-C_4-C_5$	120.5	120.5	$C_6-C_1-C_2$	121.1	119.3	$C_3-C_4-C_5$	117.4	114.7
$C_1-C_2-C_3$	118.8	119.3	$C_1-C_6-C_5$	118.7	119.1	$C_1-C_2-C_3$	119.2	120.5	$C_1-C_6-C_5$	121.2	120.5
$C_2-C_3-C_4$	120.0	119.7	$C_4-C_5-C_6$	120.0	119.9	$C_2-C_3-C_4$	122.0	122.5	$C_4-C_5-C_6$	119.0	122.5
$C_1-N_8-O_9$	118.6	117.9	$O_9-N_8-O_{10}$	122.8	124.3	$C_1-N_8-O_9$	118.2	119.3	$O_9-N_8-O_{10}$	121.3	121.3

pNA						[pNA]$^-$					
	distance (Å)			distance (Å)			distance (Å)			distance (Å)	
bond	exp	calc	bond	exp	calc	bond	exp	calc	bond	exp	calc
C_1-C_2	1.39	1.400	C_6-C_1	1.39	1.400	C_1-C_2		1.424	C_6-C_1		1.421
C_2-C_3	1.37	1.387	C_5-C_6	1.37	1.387	C_2-C_3		1.371	C_5-C_6		1.373
C_3-C_4	1.41	1.413	C_4-C_5	1.41	1.413	C_3-C_4		1.456	C_4-C_5		1.458
C_1-N_8	1.45	1.459	N_8-O_9	1.23	1.233	C_1-N_8		1.403	N_8-O_9		1.259
C_4-N_7	1.35	1.379	N_8-O_{10}	1.23	1.233	C_4-N_7		1.320	N_8-O_{10}		1.259
	angle			angle			angle			angle	
	exp	calc		exp	calc		exp	calc		exp	calc
$C_6-C_1-C_2$	122.0	120.9	$C_3-C_4-C_5$	119.0	118.9	$C_6-C_1-C_2$		118.8	$C_3-C_4-C_5$		114.6
$C_1-C_2-C_3$	119.7	119.5	$C_1-C_6-C_5$	119.7	119.5	$C_1-C_2-C_3$		120.8	$C_1-C_6-C_5$		120.7
$C_2-C_3-C_4$	120.3	120.6	$C_4-C_5-C_6$	120.3	120.6	$C_2-C_3-C_4$		122.5	$C_4-C_5-C_6$		122.6
$C_1-N_8-O_9$	118.5	118.0	$O_9-N_8-O_{10}$	123.0	124.0	$C_1-N_8-O_9$		119.5	$O_9-N_8-O_{10}$		121.1

atomic distances. The calculated (vacuum) and experimental[36−38] (solid-state) values of interatomic distances and angles are shown in Table 1. The variation of the geometric parameters with the deprotonation suggest that, in the case of the anions, a quinoid structure should be considered, because there is a shortening of the C_2-C_3 (or C_5-C_6), C_1-N_8, C_4-O_7, and C_4-N_7 bonds. In addition, there is an increase of the N−O bond lengths with a concomitant increase in the charge density at the oxygen atoms of the NO_2 moiety upon deprotonation.

Figure 2 shows the electronic spectra of pNA, pNP, and their respective anions in solution. Two common features are observed in the electronic spectra: (1) a very substantial red-shift and (2) an increase of the intensity of the electronic transitions after deprotonation. The experimental and calculated electronic transition energies, with the respective values of ground and excited-state dipole moments, are shown in Table 2.

Figure 3 displays the contours of the molecular orbitals involved in the low-energy electronic transition for the neutral and anionic species. In the case of the neutral species, one easily observes that charge density is mainly transferred from the aromatic ring to the NO_2 moiety. In the case of [pNP]$^-$, it is still possible to observe the transfer of charge density from the aromatic ring to the NO_2 moiety with significant participation of the O^- moiety. This is also supported by the values of the electric dipole moment in the ground and excited-states (Table 2). In the case of [pNA]$^-$, the corresponding values of the electric dipole moment suggest a more complex situation, because its excited-state exhibits a stronger multiconfigurational nature than those observed for the other species.

In fact, the variation in the electric dipole moment for [pNA]$^-$ (Table 2) suggests that, in this case, the NO_2 capability as an electron-withdrawing group is saturated. To further explore this point, it is convenient to analyze the Mulliken charge densities at individual atoms, as shown in Table 3 for pNP, [pNP]$^-$, pNA, and [pNA]$^-$.

Comparing the charge densities at the oxygen atoms of the NO_2 group in pNP, pNA, and the corresponding anions, one observes that, in the electronic ground state, the charge densities

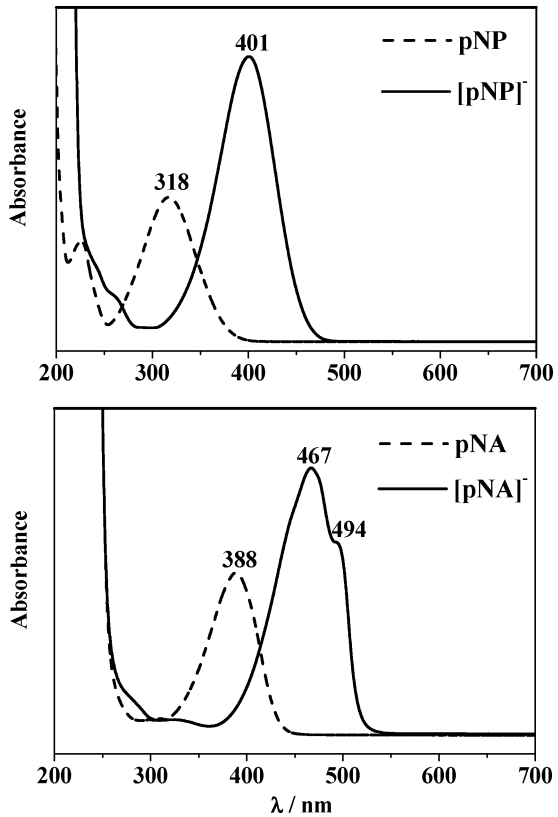

Figure 2. Electronic absorption spectra (and respective values of λ_{max} of the transitions) of neutral (---) and anionic (—) species of pNP (aqueous) and pNA (DMSO) in solution.

TABLE 2: Experimental and Calculated Vertical Excitation Energies of Neutral and Anionic Species of pNP and pNA[a]

				dipole moment (Debye)					
	E_{ge} (eV)[b]			μ_g		μ_e		$\Delta\mu_{ge}$	
molecule	exp (solution)	exp (gas)	calc	exp	calc	exp	calc	exp	calc
pNP	3.90 $\lambda_{max} = 318$ nm $\epsilon_{max} = 9000$ mol^{-1}Lcm^{-1}	4.71	4.87	4.8[c]	4.27	9.5[c]	9.81	4.7	5.54
$[pNP]^-$	3.09 $\lambda_{max} = 401$ nm $\epsilon_{max} = 19\,000$ mol^{-1}Lcm^{-1}		2.85		1.25		3.50		2.25
pNA	3.20 $\lambda_{max} = 388$ nm $\epsilon_{max} = 20\,000$ mol^{-1}Lcm^{-1}	4.24	4.32	6.2[d]	5.79	15.3[d]	14.22	9.1	8.43
$[pNA]^-$	2.65/2.51 $\lambda_{max} = 467$ nm/494 nm $\epsilon_{max} = 33\,000$ mol^{-1}Lcm^{-1}/25 000 mol^{-1}Lcm^{-1}		2.73		3.92		2.19		1.73

[a] E_{ge} is the transition energy, ϵ_{max} is the molar absorptivity, and μ_g and μ_e are the ground and excited-state dipole moments, respectively. [b] In parenthesis, the corresponding λ_{max} values. [c] Ref 14. [d] Refs 10 and 13.

TABLE 3: Mulliken Charge of Individual Atoms in Ground and Excited Electronic States of pNP, pNA, $[pNP]^-$, and $[pNA]^-$

	pNP		$[pNP]^-$		pNA		$[pNA]^-$	
atom	ground	excited	ground	excited	ground	excited	ground	excited
C_1	0.349	0.396	0.230	0.414	0.314	0.370	0.216	0.338
C_2	−0.087	−0.085	−0.108	−0.128	−0.087	−0.085	−0.087	−0.129
C_3	−0.100	−0.078	−0.145	−0.093	−0.156	−0.124	−0.125	−0.100
C_4	0.329	0.422	0.338	0.302	0.330	0.380	0.300	0.267
C_5	−0.166	−0.146	−0.170	−0.120	−0.156	−0.124	−0.190	−0.182
C_6	−0.088	−0.084	−0.102	−0.131	−0.087	−0.085	−0.085	−0.138
O_7/N_7	−0.293	−0.212	−0.605	−0.517	−0.276	−0.089	−0.512	−0.561
N_8	0.198	0.100	0.275	0.162	0.218	0.119	0.260	0.204
O_9	−0.296	−0.377	−0.455	−0.543	−0.309	−0.443	−0.538	−0.496
O_{10}	−0.294	−0.384	−0.453	−0.543	−0.310	−0.444	−0.534	−0.496

increase from pNP to $[pNP]^-$ and also from pNA to $[pNA]^-$. In the excited-state, there is again such an increase in the charge density in going from pNP to $[pNP]^-$. However, when comparing pNA and $[pNA]^-$, one observes that in the anion the charge densities at the oxygen atoms of the NO_2 group at the ground and excited-states are quite comparable. In other words, in the case of $[pNA]^-$ the charge accepting capability of the NO_2 moiety is already saturated, forcing a more homogeneous charge distribution over the molecule in the excited-state. In such a situation it would be pointless to describe the electronic transition as involving CT from the electron-donor group (NH^-) to the electron-withdrawing group (NO_2), as is the case for the neutral species.

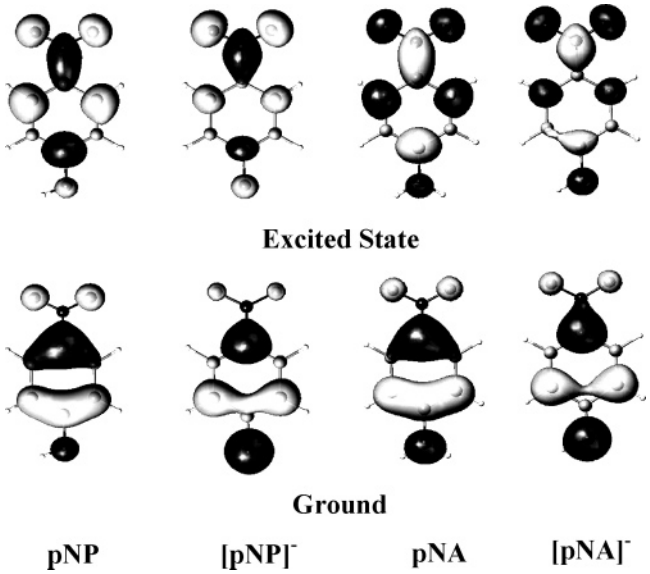

Figure 3. Contours of the molecular orbitals involved in the low-energy electronic transitions for pNP, $[pNP]^-$, pNA, and $[pNA]^-$.

The Raman spectra of pNP, pNA, and their respective anions are displayed in Figure 4. The experimental and calculated Raman frequencies for the more relevant vibrational modes, with the corresponding assignments, are shown in Table 4. As can be observed in Figure 4, the RR pattern of the neutral and anionic species shows striking differences. In the case of the neutral species, the $\nu_s(NO_2)$ is the strongest mode (ca. 1340 cm^{-1} in pNP and ca. 1310 cm^{-1} in pNA), whether at resonance or out-of-resonance. As resonance is approached in pNP, besides $\nu_s(NO_2)$ at 1340 cm^{-1}, the modes at 868 cm^{-1} (assigned to $\delta(NO_2) + \nu(CC)$), 1116 and 1173 cm^{-1} (assigned to $\delta(CH) + \nu_s(NO_2)$), 1290 cm^{-1} (assigned to $\nu(CO) + \delta(CH)$), and 1596 cm^{-1} (assigned to $\nu(CC)$) are also significantly enhanced. Similarly, in the case of pNA, besides $\nu_s(NO_2)$ at 1310 cm^{-1}, the modes at 860 cm^{-1} (assigned to $\delta(NO_2) + \nu(CC)$), 1110 and 1178 cm^{-1} (assigned to $\delta(CH) + \nu_s(NO_2)$), and 1516 cm^{-1} (assigned to $\delta(CH) + \nu(CC)$) are also significantly enhanced.

In the case of $[pNP]^-$, the modes associated with the NO_2 moiety are very substantially enhanced, such as the mode at 858 cm^{-1} (assigned to $\delta(NO_2) + \nu(CC)$) and the $\nu_s(NO_2)$, which is now shifted to 1293 cm^{-1} and whose composition also includes $\delta(CO)$ and $\delta(CH)$. The ca. 50 cm^{-1} shift to lower frequencies of the $\nu_s(NO_2)$ mode is compatible with the elongation of the N−O bond length concomitant with the shortening of the C−O bond length in the anion (Table 1). The shortening of the C−O bond length caused by deprotonation of pNP is quite noticeable, suggesting a partial double-bond character of this bond. On the other hand, the variation of the N−O bond length is relatively small, suggesting that the substantial shift of ca. 50 cm^{-1} caused by deprotonation can be traced to the coupling of the $\nu_s(NO_2)$ mode with other modes, such as $\delta(CO)$ and $\delta(CH)$ in the anion. Another important point is the great intensity of ring modes, such as 1120 and 1173 cm^{-1} (assigned to $\delta(CH) + \nu_s(NO_2)$) and the mode at 1584 cm^{-1} (assigned to $\nu(CO^-) + \nu(CC)$).

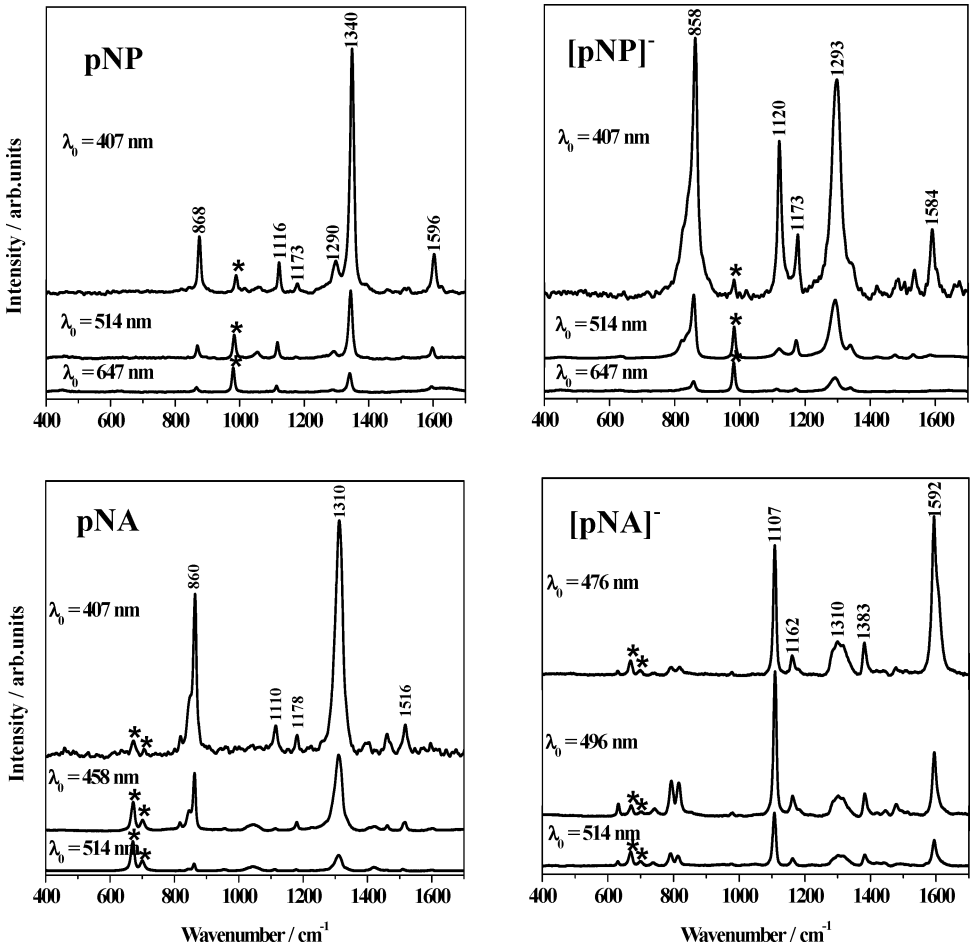

Figure 4. Raman spectra of pNP, $[pNP]^-$, pNA, and $[pNA]^-$ in different excitation energies. Internal standards: (*) 982 cm^{-1} for SO_4^{2-} and (*) 667 cm^{-1} for DMSO.

TABLE 4: Approximate Description of the Most Relevant Raman Modes (Experimental and Calculated Frequencies) of pNA, pNP, $[pNA]^-$, and $[pNP]^-$

Raman shift/cm^{-1}								
pNP		$[pNP]^-$		pNA		$[pNA]^-$		
exp	calc	exp	calc	exp	calc	exp	calc	assignment
868	874	858	838	860	872	815	834	$\delta(NO_2)$, ν(CC)
1116	1115	1120	1128	1110	1128	1107	1130	δ(CH), $\nu_s(NO_2)$
1173	1184	1173	1181	1178	1197	1162	1173	δ(CH), $\nu_s(NO_2)$
1290	1290		1257					ν(CO)
		1293						$\nu_s(NO_2)$, δ(CH), δ(CO)
1340	1376		1340	1310	1370		1348	$\nu_s(NO_2)$
		1531	1547	1516	1526			ν(CC), δ(CH)
		1584	1578					ν(CC), ν(CO)
						1592	1545	ν(CC), ν(CN)
1596	1584							ν(CC), δ(CH)

In the case of $[pNA]^-$, a striking difference of the RR pattern is observed in comparison to $[pNP]^-$. A landmark of the Raman spectra of nitroaromatics is the presence of a very strong band in the 1300−1350 cm^{-1} region. In the Raman spectrum of $[pNA]^-$, a weak and broad band is observed at ca. 1310 cm^{-1}, and it is difficult to assign this band to $\nu_s(NO_2)$ because the calculations predict a frequency shift of ca. 22 cm^{-1} to lower wavenumbers of this mode with the deprotonation. Obviously, the comparison of our experimental and calculated values is not straightforward, because the calculations were performed for the molecule in vacuum. The situation here is in fact much more complex because the assignment of the $\nu_s(NO_2)$ is highly controversial, even for the neutral species.[3,4,39−43] In fact, this mode is rather sensitive to the solvent, shifting from 1340 cm^{-1} in hexane to ca. 1310 cm^{-1} in DMSO.[3] In the present paper, we assume that the $\nu_s(NO_2)$ in $[pNA]^-$ is redistributed into lower frequency modes, with a significant contribution to the mode at ca. 1107 cm^{-1}, due to its resonance enhancement behavior.

The RR spectra of $[pNA]^-$ show the substantial enhancement of the modes at 1107 and 1592 cm^{-1}. The band at ca. 1107 cm^{-1} is assigned to δ(CH) + $\nu_s(NO_2)$, and the band at ca. 1592 cm^{-1} is assigned to a ring mode involving the quinoid ν(CC) + ν(CN) stretchings. When we examine the electronic spectrum (Figure 2) of $[pNA]^-$, one observes a rather strong band at ca. 467 nm and a shoulder at ca. 494 nm. The Raman spectra excited close to these maxima show the preferential enhancement of different modes, that is, the ring mode at 1592 cm^{-1} and the band at 1107 cm^{-1}, respectively. The difference within the two maxima corresponds to ca. 1170 cm^{-1}, which strongly suggests that the observed shoulder is in fact a vibronic component involving the mode at 1107 cm^{-1}. It is well-known that, within the Franck−Condon approximation, the progression generating mode is the one that involves a substantial change in geometry, which is consistent with the participation of the NO_2 moiety in the 1107 cm^{-1} mode.

4. Conclusions

The analysis of the RR spectra of pNP, pNA, and their respective anions, supported by quantum-chemical calculations, reveals qualitative differences concerning the electron-withdrawing capability of the NO_2 group, depending on the nature of the group in the para-position relative to the NO_2 moiety. In the case of pNP, the deprotonation leads to the anionic species

$[pNP]^-$, where the NO_2 moiety becomes a better electron-acceptor group as compared to the neutral species. This is confirmed by the nature of the molecular orbitals involved in the CT resonant transition and by the substantial enhancement of the modes associated with the NO_2 moiety of the anion. In the case of the $[pNA]^-$ species, the situation is much more complex, because the enhancement of the NO_2 modes generally observed in the RR spectra is not observed at all. It is suggested that the rationale for this behavior is related to the saturation of the electron-withdrawing capability of the NO_2 moiety in $[pNA]^-$ in the ground state, which in turn leads to rather small variations in the N−O bond length in the excited-state. In other words, in the case of $[pNA]^-$, the transition is much more delocalized over the whole molecule, as confirmed by the RR pattern that now shows expressive enhancement of ring modes.

Acknowledgment. The authors are indebted to Fundação de Amparo à Pesquisa do Estado de São Paulo (FAPESP), Conselho Nacional de Desenvolvimento Científico e Tecnológico (CNPq), and Instituto do Milènio de Materiais Complexos (IMMC) for financial support and to the Laboratório de Computação Científica Avançada (LCCA) of the Universidade de São Paulo for the services and computer time.

References and Notes

(1) Behringer, J. *Raman Spectroscopy − Theory and Practice*; Szymanski, H. A. Ed.; Plenum Press: New York, 1967; Vol. 1, p 168.

(2) Kumar, K.; Carey P. R. *J. Chem. Phys.* **1975**, *63*, 3697.

(3) Schmid, E. D.; Moschallski, M.; Peticolas, W. L. *J. Phys. Chem.* **1986**, *90* (11), 2340.

(4) Moran, A. M.; Kelley, A. M. *J. Chem. Phys.* **2001**, *115*, 912.

(5) Prasad, P. N.; Williams D. J. *Introduction to Nonlinear Optical Effects in Molecules and Polymers*; John Wiley & Sons: New York, 1991; p 135.

(6) Painelli, A. *Synth. Met.* **1999**, *101*, 218.

(7) Muthuraman, M.; Masse R.; Nicoud, J. F.; Desiraju, G. R. *Chem. Mater.* **2001**, *13*, 1473.

(8) Panunto, T. W.; Urbánczyk-Lipkowska Jonhson, R.; Etter, M. C. *J. Am. Chem. Soc.* **1987**, *109*, 7786.

(9) Castiglioni, C.; Del Zoppo, M.; Zerbi, G. *Phys. Rev. B* **1996**, *53* (20), 13319.

(10) Scalmani, G.; Frisch M. J.; Mennucci B.; Tomasi J.; Cammi R; Barone V. *J. Chem. Phys.* **2006**, *124* (9), 094107.

(11) Sinha, H. K.; Yates, K. *Can. J. Chem.* **1991**, *69*, 550.

(12) Sinha, H. K.; Yates, K. *J. Am. Chem. Soc.* **1991**, *113*, 6062.

(13) Wortmann, R.; Kramer, P.; Glania, C.; Lebus, S.; Detzer, N. *Chem. Phys.* **1993**, *173*, 99.

(14) Prabhu Mirashi, L. S.; Kunte, S. S. *Spectrochim. Acta* **1989**, *45A* (11), 1147.

(15) Cammi, R.; Frediani, L.; Menucci, B.; Ruud, K. *J. Chem. Phys.* **2003**, *119* (12), 5818.

(16) Farztdinov, V. M.; Schanz, R.; Kovalenko, A.; Ernsting, N. P. *J. Phys. Chem. A* **2000**, *104*, 1486.

(17) Clark, R. J. H.; Dines, T. J. *Angew. Chem., Int. Ed. Engl.* **1986**, *25*, 131.

(18) Schulman, S. G.; Vincent, W. R.; Underberg, W. J. M. *J. Phys. Chem.* **1981**, *85*, 4068.

(19) Muniz-Miranda, M. *J. Raman Spectrosc.* **1997**, *28*, 205.

(20) Stewart, R.; Dolman, D. *Can. J. Chem.* **1967**, *45*, 925.

(21) Cox, R. A.; Stewart, R. *J. Am. Chem. Soc.* **1976**, *98* (2), 488.

(22) Becke, A. D. *J. Chem. Phys.* **1993**, *98*, 5648.

(23) Lee, C.; Yang, W.; Parr, R. G. *Phys. Rev. B* **1988**, 37, 785. Stephens, P. J.; Devlin, F. J.; Chabalowski, C. F.; Frish, M. J. *J. Phys. Chem.* **1994**, *98*, 11623.

(24) Kendall, R. A.; Dunning, T. H., Jr.; Harrison, R. J. *J. Chem. Phys.* **1992**, *96*, 6796.

(25) Frisch, M. J.; Trucks, G. W.; Schlegel, H. B.; Scuseria, G. E.; Robb, M. A.; Cheeseman, J. R.; Montgomery, J. A., Jr.; Vreven, T.; Kudin, K. N.; Burant, J. C.; Millam, J. M.; Iyengar, S. S.; Tomasi, J.; Barone, V.; Mennucci, B.; Cossi, M.; Scalmani, G.; Rega, N.; Petersson, G. A.; Nakatsuji, H.; Hada, M.; Ehara, M.; Toyota, K.; Fukuda, R.; Hasegawa, J.; Ishida, M.; Nakajima, T.; Honda, Y.; Kitao, O.; Nakai, H.; Klene, M.; Li, X.; Knox, J. E.; Hratchian, H. P.; Cross, J. B.; Bakken, V.; Adamo, C.; Jaramillo, J.; Gomperts, R.; Stratmann, R. E.; Yazyev, O.; Austin, A. J.; Cammi, R.; Pomelli, C.; Ochterski, J. W.; Ayala, P. Y.; Morokuma, K.; Voth, G. A.; Salvador, P.; Dannenberg, J. J.; Zakrzewski, V. G.; Dapprich, S.; Daniels, A. D.; Strain, M. C.; Farkas, O.; Malick, D. K.; Rabuck, A. D.; Raghavachari, K.; Foresman, J. B.; Ortiz, J. V.; Cui, Q.; Baboul, A. G.; Clifford, S.; Cioslowski, J.; Stefanov, B. B.; Liu, G.; Liashenko, A.; Piskorz, P.; Komaromi, I.; Martin, R. L.; Fox, D. J.; Keith, T.; Al-Laham, M. A.; Peng, C. Y.; Nanayakkara, A.; Challacombe, M.; Gill, P. M. W.; Johnson, B.; Chen, W.; Wong, M. W.; Gonzalez, C.; Pople, J. A. *Gaussian 03*, Revision D.01; Gaussian, Inc.: Wallingford, Connecticut, 2004.

(26) Roos, B. O. In *Advances in Chemical Physics; Ab Initio Methods in Quantum Chemistry - II*; Lawley, K. P., Ed.; John Wiley & Sons: Chichester, 1987.

(27) Andersson, K.; Malmqvist, P.-Å.; Roos, B. O.; Sadlej, A. J.; Wolinski, K. *J. Phys. Chem.* **1990**, *94*, 5483.

(28) Andersson, K.; Malmqvist, P.-Å.; Roos, B. O. *J. Chem. Phys.* **1992**, *96*, 1218.

(29) Ghigo, G.; Roos, B. O.; Malmqvist, P.-Å.; *Chem. Phys. Lett.* **2004**, *396*, 142.

(30) Widmark, P.-O.; Malmqvist, P.-Å.; Roos. B. O. *Theor. Chim. Acta* **1990**, *77*, 291.

(31) Roos. B. O.; Fülscher, M. P.; Malmqvist, P.-Å.; Merchán, M.; Serrano-Andrés, L. In *Quantum Mechanical Electronic Structure Calculations with Chemical Accuracy*; Langhoff. S. R., Ed.; Kluwer Academic: Dordrecht, The Netherlands, 1995.

(32) Roos, B. O.; Borin, A. C.; Gagliardi, L. *Angew. Chem., Int. Ed.* **2007**, *46*, 1469.

(33) Serrano-Andrés, L.; Merchán, M.; Borin, A. C. *Proc. Nat. Acad. Sci.* **2006**, *103*, 8691.

(34) Forsberg, N.; Malmqvist, P.-Å. *Chem. Phys. Lett.* **1997**, *274*, 196.

(35) Karlström, G.; Lindh, R.; Malmqvist, P. Å.; Roos, B. O.; Ryde, U.; Veryazov, V.; Widmark, P. O.; Cossi, M.; Schimmelpfennig, B.; Neogrady, P.; Seijo, L. *Comput. Mater. Sci.* **2003**, *28*, 222.

(36) (a) Coppens, P.; Schimdt, G. M. J. *Acta Crystallogr.* **1965**, *18*, 62, (b) 654.

(37) Minemoto, H.; Sonoda, N. *Acta Crystallogr.* **1992**, *C48*, 737.

(38) Trueblood, K. N.; Goldish, E.; Donohue, J. *Acta Crystallogr.* **1961**, *14*, 1009.

(39) Harrand, M. *J. Raman Spectrosc.* **1975**, *4*, 53.

(40) Harrand, M. *J. Raman Spectrosc.* **1979**, *8* (3), 161.

(41) Bertrán, J. F.; Hernández, M.; La Serna, B. *Spectrochim. Acta A* **1982**, *38* (2), 149.

(42) Epstein, L. M.; Shubina, E. S.; Ashkinadze, L. D.; Kazitsyna, L. A. *Spectrochim. Acta A* **1982**, *38* (3), 317.

(43) Fujisawa, T.; Terazima, M.; Kimura, Y.; Maroncelli, M. *Chem. Phys. Lett.* **2006**, *430*, 303.